Baltic Astronomy, vol. 14, 535–542, 2005.

DYNAMICAL FACTORS DESTROYING REGULAR MOTION IN BARRED GALAXIES

N. D. Caranicolas and N. J. Papadopoulos

Department of Physics, Section of Astrophysics, Astronomy and Mechanics, University of Thessaloniki, 541 24 Thessaloniki, Greece

Received: 2005 October 4; revised 2005 November 25

Abstract. We study the behavior of orbits in a barred galaxy model composed of an harmonic oscillator potential plus a potential of a dense nucleus. The presence of a small mass nucleus destroys the figure-eight orbits which turn gradually to elongated box orbits supporting the bar. For larger values of the nucleus mass the majority of orbits become chaotic. It is shown that the percentage of chaotic orbits increases as the nucleus mass increases. The chaotic region also increases as the angular velocity increases. A connection between the angular velocity and angular momentum is presented. All numerical calculations strongly suggest that orbits with large average values of angular momentum remain regular. Comparison to previous work shows that the present results show similarities with those obtained for axially symmetrical galaxies.

Key words: galaxies: kinematics and dynamics – galaxies: nuclei

1. INTRODUCTION

Recent observations by ground based telescopes with adaptive optics and the Hubble Space Telescope (HST) suggest that about 2/3 of disk galaxies show a barred structure. Furthermore, on scales smaller than 1 kpc, more than 50 % of them host secondary bars (see Lauricainen, Salo & Buta 2004 and references therein).

The properties of orbits in two-dimensional barred galaxy models have been studied for many years, and a large number of articles has been published that is too numerous to cite individually. Interesting reviews can be found in Contopoulos & Grosbøl (1989), Bosma (1992), Sellwood & Wilkinson (1993), Martinet (1995), Freeman (1996).

In this paper we shall study the motion in the potential

$$V(x,y) = \frac{\alpha}{2}(x^2 + 4y^2) - \frac{M_n}{(x^2 + y^2 + c_n^2)^{1/2}} \quad . \tag{1}$$

The two dimensional potential (1) was chosen because, we believe, that it is a good approximation for the system described, i.e., central parts of a barred galaxy. As one can see, it consists of two parts. The first part is a two-dimensional harmonic oscillator, α being a parameter. This potential is based on the figure-eight orbits which support a barred structure and can be found using the theory of the inverse problem (see Bozis 1995; Bozis & Borgero 1997; Bozis & Kotoulas

2004; Caranicolas 1998; Caranicolas & Karanis 1998). The second part represents the potential of a nucleus of mass M_n and scale-length c_n. Therefore, potential (1) can be considered to represent a nuclear bar. We have chosen this potential for several reasons. The first reason is to investigate the properties of motion in the barred galaxy potential (1), which is the sum of two integrable potentials. The second reason is to see how the two basic factors, i.e., the nucleus mass and the angular velocity affects the character of motion (regular or chaotic). A third reason is to follow the evolution of the basic family of orbits, i.e., the figure-eight orbits, as the above physical parameters change. Another interesting point of view is to seek for physical quantities playing a critical role on the regular or chaotic nature of orbits. Such an interesting physical quantity is the angular momentum. A new aspect of this study, that makes things more interesting, is that the angular momentum, is not conserved for the potential (1).

Assuming a clockwise rotation at the constant angular velocity Ω, we can describe the motion by the Hamiltonian,

$$H_J = \frac{1}{2}(p_x^2 + p_y^2) + V(x,y) - \frac{1}{2}\Omega^2(x^2+y^2) = \frac{1}{2}(p_x^2+p_y^2) + V_{\text{eff}}(x,y) = E_J \quad , \quad (2)$$

where p_x, p_y are the momenta per unit mass, conjugate to x and y, while $V_{\text{eff}}(x,y)$ is the effective potential

$$V_{\text{eff}}(x,y) = V(x,y) - \frac{1}{2}\Omega^2(x^2+y^2) \quad . \quad (3)$$

This Hamiltonian is the well known Jacobi integral and E_J is its numerical value.

We use a system of galactic units, where the unit of length is 1 kpc, the unit of time is 0.97746×10^8 yr and the unit of mass is $2.325\times10^7 M_\odot$. The velocity and the angular velocity units are 10 km/s and 10 km/s/kpc respectively, while G is equal to unity. The energy unit (per unit mass) is 100 (km/s)^2. In these units, we take $\alpha = 100$ km/s/kpc, $c_n = 0.25$ kpc, while M_n and Ω are treated as parameters.

Our study is based on the numerical integration of the equation of motion

$$\ddot{x} = -2\Omega\dot{y} - \frac{\partial V_{\text{eff}}}{\partial x} \ , \ \ddot{y} = 2\Omega\dot{x} - \frac{\partial V_{\text{eff}}}{\partial y} \quad , \quad (4)$$

where the dot indicates derivative with respect to the time. In Section 2 we study the properties of motion in the non-rotating potential. The motion in the rotating potential is presented in Section 3. Section 4 is devoted to the discussion and conclusions of this work.

2. MOTION IN THE NON-ROTATING POTENTIAL

In order to obtain a complete picture of the properties of motion in the Hamiltonian (2) we shall start from the case $\Omega = 0$. The very useful tool of the $x - p_x, y = 0, p_y > 0$ *Poincaré* surface of section allows one to visualize the properties of motion and to locate the main families of orbits in the system. Fig. 1 shows the structure of the surface of a section when $E_J = 250, M_n = 400$. One can see a large chaotic region as well as regions, where the motion is regular. Fig. 2 shows four typical orbits. Fig. 2a shows an orbit forming two of the four big islands shown in Fig. 1, while Fig. 2b shows an orbit symmetrical to Fig. 2a

and forming the other two big islands. As one can see, these orbits support the bar structure. Fig. 2c shows a tube orbit, which stays close to the nearly circular stable periodic orbit. This kind of orbits support the central mass concentration. Fig. 2d shows a chaotic orbit. The bar-shape of this orbit is evident. Therefore, in the case where a massive nucleus is present, our numerical calculations suggest that we have a bar structure made of a mixture of regular and chaotic orbits.

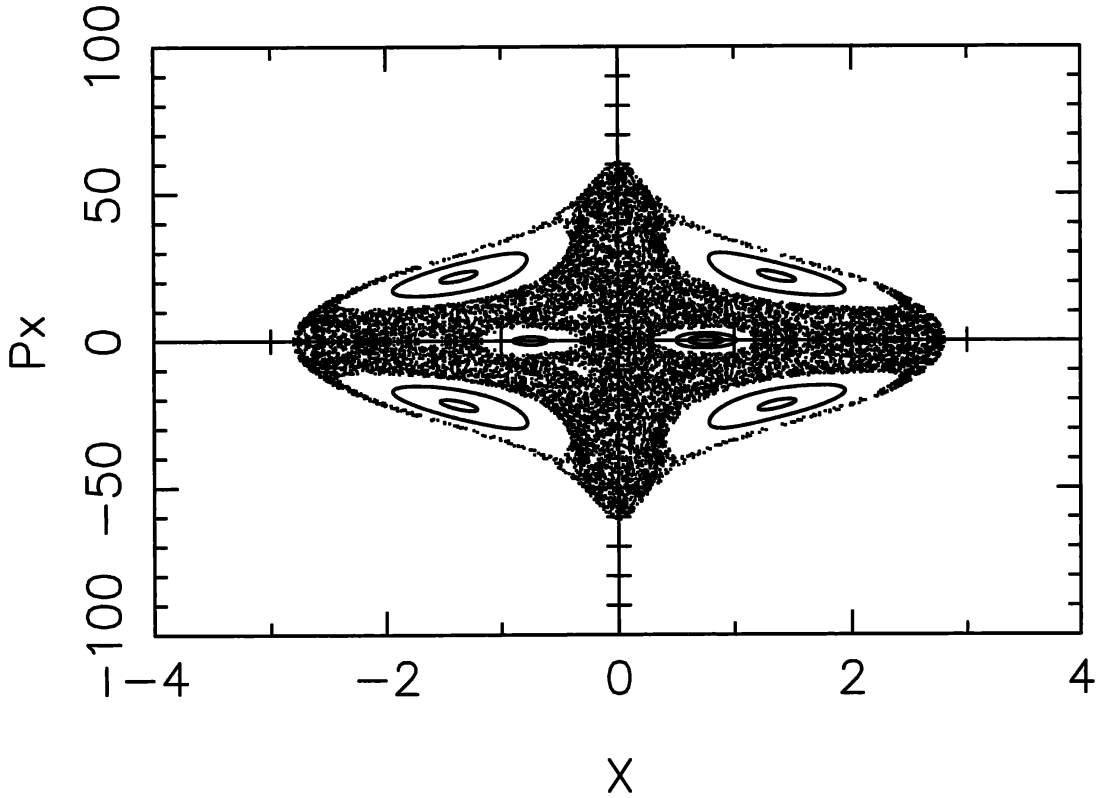

Fig. 1. The $x - p_x$ surface of section for the Hamiltonian (2), when $E_J = 250$, $M_n = 400$, $\Omega = 0$, $\alpha = 100$, $c_n = 0.25$. A large part of the phase plane is covered by chaotic orbits.

An illustrative example is the evolution of the figure-eight orbits, which are the basic orbits in the absence of the nucleus. Fig. 3a shows the shape of such an orbit when $M_n = 5$, after 3×10^8 yr. We see that the orbit retains its shape for small time periods. Fig. 3b shows the same orbit after 2×10^9 yr. Now the orbit has become a box orbit but its figure-eight origin is evident. For larger values of mass of nucleus the figure-eight orbits evolve to chaotic orbits. The reason for that will be analyzed in the next Section.

It is of interest to follow the evolution of the regular region on the $x - p_x$ surface of section vs. the mass of the nucleus (i.e., the percentage of the surface of section covered by regular orbits as a function of the mass of the nucleus). Such a plot is shown in Fig. 4. Note that, when $M_n = 0$, the potential is integrable and all orbits are periodic figure-eight orbits. As the mass of nucleus increases, the regular region decreases rapidly and chaotic regions appear. For larger values of the mass of nucleus the regular region decreases asymptotically.

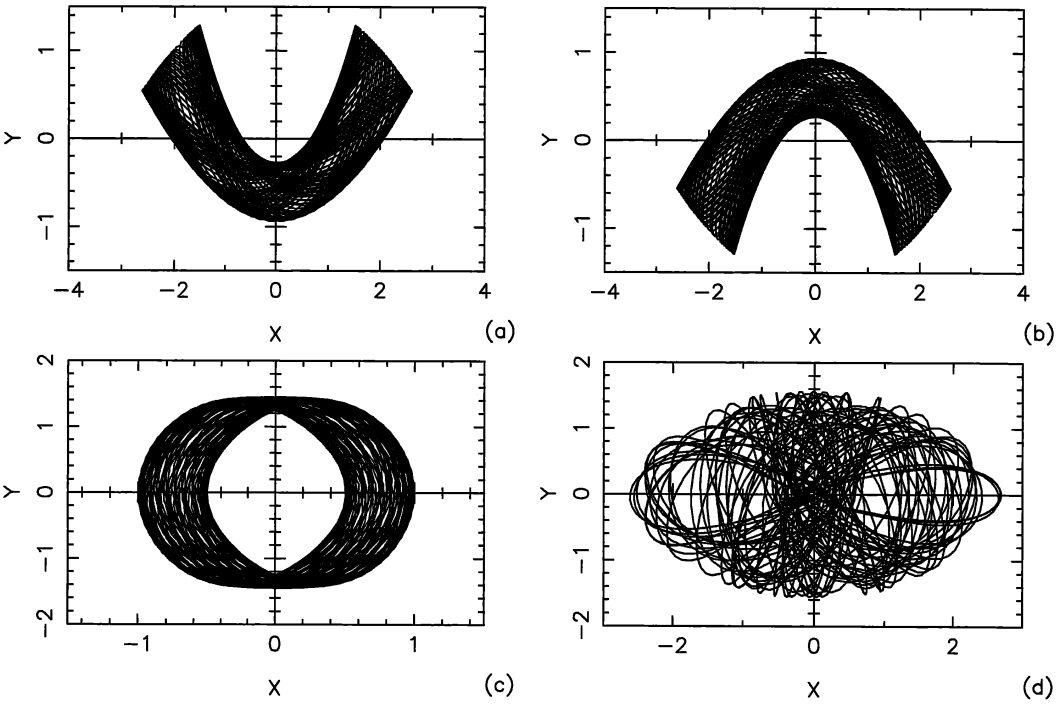

Fig. 2. Typical orbits in the Hamiltonian (2). The values of parameters are the same as in Fig. 1.

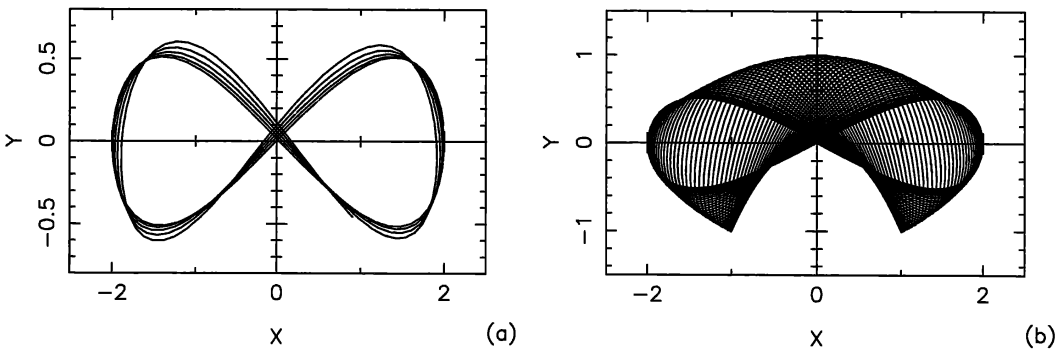

Fig. 3. Evolution of a figure-eight orbit in the non-rotating potential, $M_n = 5$, while the values of parameters are the same as in Fig. 1.

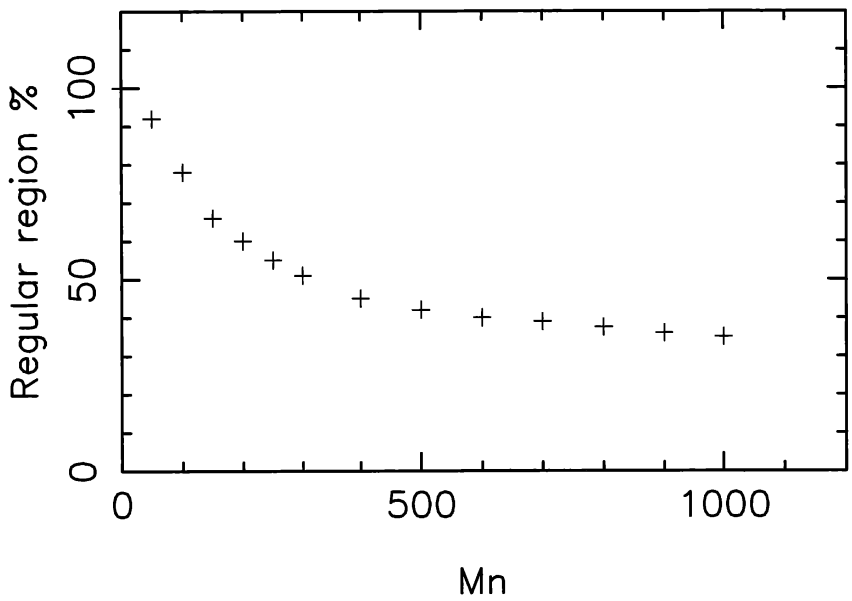

Fig. 4. A plot of the evolution of the regular region vs M_n. The regular region decreases as the mass of the nucleus increases.

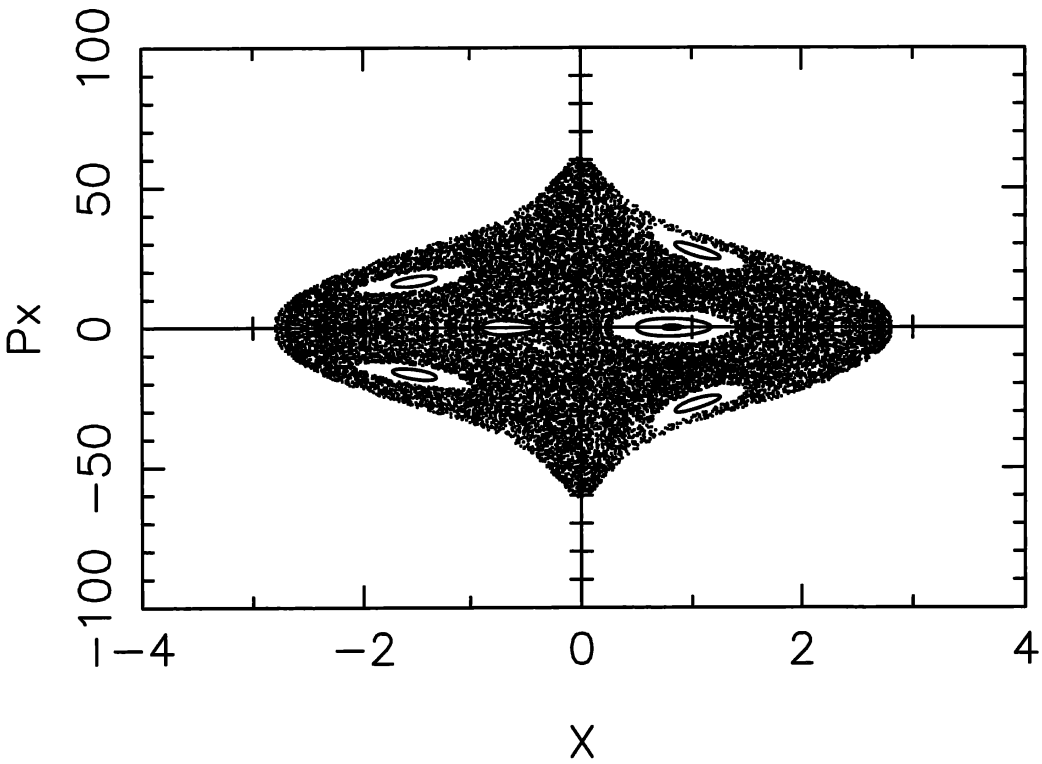

Fig. 5. The $x - p_x$ surface of section for the Hamiltonian when $\Omega = 1.25$. The values of other parameters are the same as in Fig. 1. Note that the chaotic region is larger than that of Fig. 1.

Thus, in the case of the non-rotating potential, our numerical outcomes lead to the following conclusion: when $M_n = 0$, we have a bar structure based on the figure-eight orbits, which, as the mass of nucleus increases, is not destroyed but it maintains its shape, which is now based on both regular and chaotic orbits shown in Fig. 2.

3. MOTION IN THE ROTATING POTENTIAL AND THE ROLE OF ANGULAR MOMENTUM

Let us now analyze the motion when the bar rotates, i.e., the case when $\Omega \neq 0$. The $x - p_x$ *Poincaré* surface of section of the system, when $\Omega = 1.25$, is shown in Fig. 5. The values of the parameters and energy are the same as in Fig. 1. It is evident that the phase plane of Fig. 5 is similar to that of Fig. 1 with the same families of orbits. The only difference is that in this case the chaotic region has increased. As all the parameters and the energy are the same as in Fig. 1, we come to the conclusion that the increase of the chaotic region is due to the bar's rotation. Results, not shown here, indicate that, when Ω increases, the chaotic region increases too, when the other parameters are kept constant.

This phenomenon seems to be of interest and it would be nice to investigate it further. A good point to start up is to see what happens with the angular momentum of different families of orbits. The expression giving the angular momentum in the rotating potential (3) is

$$L = x\dot{y} - y\dot{x} - \Omega(x^2 + y^2) \quad . \tag{5}$$

The above expression indicates that the value of the angular momentum decreases as Ω increases. Therefore, if all other parameters are kept constant, the decrease of L will be responsible for the increase of chaotic regions. Of course, the angular momentum is not conserved but we can take the plot of the angular momentum L vs. time t and try to get some conclusions.

Such a plot is shown in Figures 6a-d. In Fig. 6a we see the $L - t$ diagram for the figure-eight orbit shown in Fig. 3 for 2×10^9 yr. On a complete empirical basis we can say that the average value $< L >$ of the angular momentum for that orbit is around zero. In order to be sure, we can compute $< L >$ numerically by the formula

$$< L >= \sum_{i=1}^{n} L_i \quad . \tag{6}$$

For a time period of 2×10^9 yr we use the value $n = 400$ for a regular orbit, while for chaotic orbits we take $n = 2000$. For the above figure-eight orbit, from (6) we find $< L >= -0.23$, close to the empirical estimated value. Fig. 6b shows the same orbit when $\Omega = 1.25$. Here we see that the average value of L is smaller and negative. Equation (6) gives $< L >= -5.2$. Therefore, the decrease of angular momentum with Ω is verified numerically. Fig. 3d shows the same diagram for a chaotic orbit, when $M_n = 400, \Omega = 2.25$, while the values of all other parameters are as in Fig. 1. Here we see that the value of L undergoes abrupt changes, while the average value is even smaller. Here we find $< L >= -5.5$. Things are completely different in Fig. 6d where we can see small changes on L which has a positive average value $< L >= 25.8$. This diagram belongs to a regular orbit starting near the stable retrograde periodic orbit giving the set of small islands

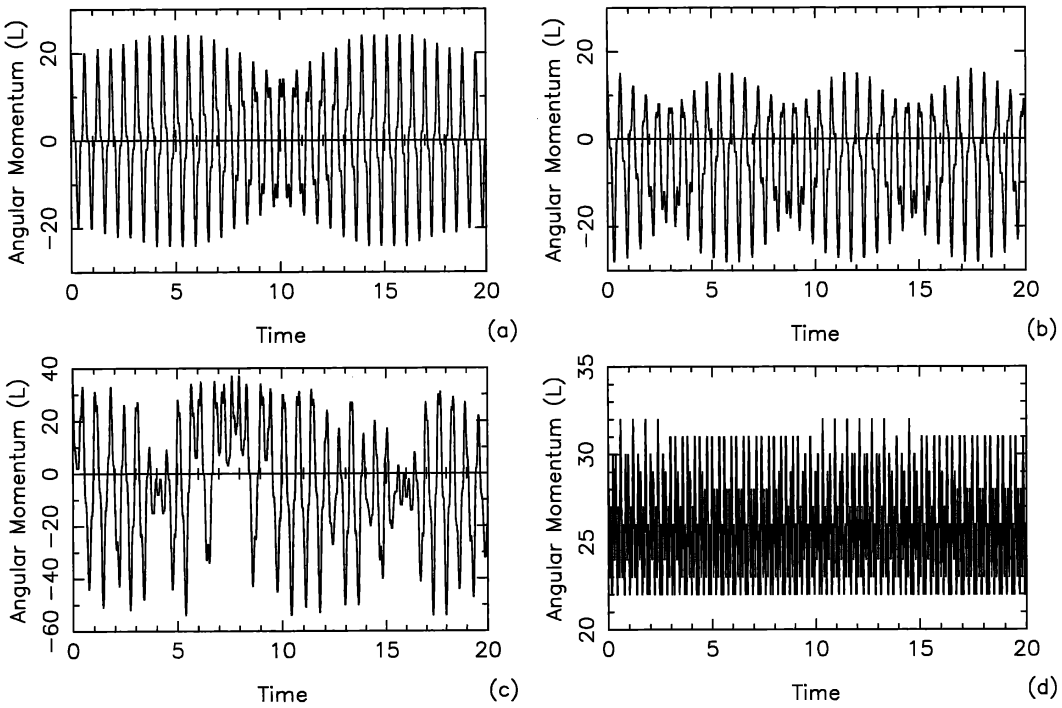

Fig. 6. Evolution of the angular momentum vs. time. Details are given in text.

on the right-hand side of Fig. 5. The initial conditions are $x = 1.0, p_x = 0$. The values of all other parameters are as in Fig. 5 and $\Omega = 2.25$.

The above analysis indicates that the angular momentum plays a significant role on the orbits of regular or chaotic character in galaxies with dense nuclei. Of course, this result was already known for about two decades (see Carlberg & Innanen 1987; Caranicolas & Innanen 1990). What is new here, is that this important phenomenon is observed not only in the case when the angular momentum is conserved, but also in cases, when the angular momentum is variable. In other words, the angular momentum plays an important role in the presence of chaos, both in the axially symmetrical and in the bar galaxies with massive nuclei.

4. DISCUSSION AND CONCLUSIONS

In the present article we have studied the motion in a potential describing central parts of a barred galaxy. The barred structure is described by a harmonic oscillator potential to which we add a dense nucleus. The presence of the dense nucleus destroys the figure-eight orbits and builds up a barred structure, based on both regular and chaotic orbits, as the mass of nucleus increases. The above results support another aspect, different from that given by recent two-dimensional studies in barred models, where the bar structure was primarily supported by quasi-periodic orbits (see Contopoulos 2002; Kaufmann & Patsis 2005).

The percentage of chaotic orbits increases as the angular velocity of the bar increases. The analysis of this interesting phenomenon shows that the angular momentum decreases as Ω increases. This outcome leads to the conclusion that the low angular momentum stars suffer chaotic motion not only in the cases when the angular momentum is conserved but also in cases when the angular momentum

is not conserved. In this latter case, the average value $< L >$ of the angular momentum is used.

The results of this work are completely different compared with the outcomes found in the work of Caranicolas & Karanis (1998), where the decrease of the chaotic regions occurred as Ω increased. This was explained that the increase of Ω has led to the decrease in the escape perturbation parameter, while the angular momentum was not involved. However, it was difficult to obtain a theoretical connection of the angular momentum with the escape perturbation parameters. We hope to be able to do this in future, using a suitable local potential made by perturbed harmonic oscillators (see Innanen 1985; Caranicolas 1990; Elipe & Deprit 1999).

A general conclusion achieved in this and in our previous studies is that both in the axially-symmetrical and barred galaxies, having dense and massive nuclei, the low angular momentum stars are subject to chaotic motions.

ACKNOWLEDGMENTS. The authors would like to thank the referee for helpful comments and suggestions that improved the quality of the paper.

REFERENCES

Bosma A. 1992, in *Morphological and Physical Classification of Galaxies*, eds. G. Longo, M. Cappaccioli & G. Busarello, Kluwer Academic Publishers, Dordrecht, p. 207

Bozis G. 1995, Inverse Problems, 11, 687

Bozis G., Borgero F. 1997, *Potenziali compatibili con famiglie di orbite date in forma parametrica*, in XIII Congresso Nationale Associaziona Italiana di Meccanica Teoreca Applicata, Siena, ed. P. Villagio

Bozis G., Kotoulas Th. 2004, Rendiconti Seminario Facoltà Scienze, Università Cagliari, 74, 83

Caranicolas N. D. 1990, Cel. Mech., 47, 87

Caranicolas N. D. 1998, A&A, 332, 88

Caranicolas N. D., Innanen K. A. 1991, AJ, 102, 1043

Caranicolas N. D., Karanis G. I. 1998, A&SS, 259, 45

Carlberg R. G., Innanen K. A. 1987, AJ, 94, 666

Contopoulos G. 2002, *Order and Chaos in Dynamical Astronomy*, Springer, Berlin

Contopoulos G., Grosbøl P. 1989, A&A, 155, 11

Elipe A., Deprit A. 1999, Mech. Res. Com., 26, 635

Freeman K. C. 1996, in *Barred Galaxies*, eds. R. Buta, D. A. Crocker, B. G. Elmegreen, ASP Conf. Ser., 91, 1

Innanen K. A. 1985, AJ, 90, 2387

Kaufmann D. E., Patsis P. 2005, AJ, 624, 693

Lauricainen E., Salo H., Buta R. 2004, AJ, 607, 103

Martinet L. 1995, Funtamentals of Cosmic Physics, 15, 351

Sellwood J. A., Wilkinson A. 1993, Rep. Prog. Phys., 56, 173